Journal of Alloys and Compounds 480 (2009) 674–680

Contents lists available at ScienceDirect

Journal of Alloys and Compounds

journal homepage: www.elsevier.com/locate/jallcom

Synthesis and electromagnetic wave absorption property of Ni–Ag alloy nanoparticles

Chung-Che Lee, Ya-Yi Cheng, Hsiang Yu Chang, Dong-Hwang Chen*

Department of Chemical Engineering, National Cheng Kung University, Tainan 701, Taiwan

ARTICLE INFO

Article history:
Received 6 November 2008
Received in revised form 3 February 2009
Accepted 3 February 2009
Available online 20 February 2009

Keywords:
Metals and alloys
Nanostructured materials
Composite materials
Chemical synthesis
Microstructure

ABSTRACT

Ni–Ag alloy nanoparticles with various molar ratios were synthesized and embedded in the epoxy for the investigation of electromagnetic wave absorption properties in 2–40 GHz. The reflection loss measurement indicated Ni nanoparticles had a significant absorption in 18–40 GHz while no significant absorption was observed in the whole frequency range examined for Ag nanoparticles. Ni_1Ag_1 nanoparticles exhibited a significant absorption as Ni nanoparticles did, but the absorption frequency range shifted from 18–40 to 2–18 GHz. Interestingly and notably, both the Ni_3Ag_1 and Ni_1Ag_3 nanoparticles showed dual-frequency absorption in 2–18 and 18–40 GHz. It was suggested that the Ni- and Ag-rich microdomains might be formed within the Ni_3Ag_1 and Ni_1Ag_3 nanoparticles, leading to the appearance of the second absorption due to the lags of polarization at the interfaces as the frequency was varied. The composition-related microstructure also affected the permittivity and permeability more significantly than the composition itself.

1. Introduction

Because of the advantage of large data transmission, various electronic and communication devices using the electromagnetic (EM) wave in the range of 1–40 GHz are being developed rapidly in the recent years [1]. For the normal operation of devices and human health, the development of the corresponding EM wave absorbers becomes more and more important [2,3]. In general, the shielding efficiency of EM wave absorbers depends on the matching frequency, layer thickness of absorbers, and the relative complex permeability and permittivity of the fillers which are determined by their nature, shape, size, and microstructure [2,4,5]. Owing to the high Snoek's limit, metallic soft magnetic materials may be more suitable as the microwave absorbers in the frequency range over gigahertz compared to the conventional ferrites [4,5]. However, to avoid the decrease of the relative complex permeability due to the eddy current loss, the metallic particles must be isolated with size less than the skin depth [4,5]. So, the studies on the metallic magnetic sub-micro particles and nanocomposites embedded in the non-conductive matrixes for the EM wave absorption received increasingly attention in recent years [1,2,4,5].

Due to the rapid development of science and technology, now the EM wave absorbers are further required to possess more advantages such as light-weight and thinness, wide absorption frequency, multi-frequency absorption, high thermal stability, and anti-oxidation. Metal magnetic nanoparticles may be quite suitable as EM wave absorbers because of their small size, large specific surface area, high surface atom percentage and more dangling chemical bonds, which might lead to the interface polarization and the activation of nanoparticles. However, each kind of metal magnetic nanoparticles has its intrinsic properties and usually can be used only in a specified frequency range. To meet the above requirements, the development of composite metal nanoparticles which combine two or more components in each individual particle to modify the bulk properties [6–11] or the surface properties may be an efficient strategy [12–20].

Ni is an important soft magnetic metal and Ag is known to possess high electric conductivity. Their combination as an EM wave absorber may be interesting. Recently we have prepared Ni, Ag, and Ni–Ag core–shell nanoparticles by various methods [21–25], and found that Ni–Ag core–shell nanoparticles showed a novel dual-frequency absorption property in 2–18 and 18–40 GHz although Ni nanoparticles exhibited absorption only in 18–40 GHz and no absorption was observed for Ag nanoparticles in 2–40 GHz [26]. The additional absorption of Ni–Ag core–shell nanoparticles in 2–18 GHz was attributed to the lags of polarization between the core/shell interfaces as the frequency was varied, which contributed to the dielectric loss [5,26]. Compared to the core–shell nanoparticles, alloy nanoparticles are relatively easily synthesized

* Corresponding author at: National Cheng Kung University, Department of Chemical Engineering, No 1, Ta-Hsueh Rd, Taiwan 701,Taiwan.
Tel.: +886 6 2757575x62680; fax: +886 6 2344496.
E-mail address: chendh@mail.ncku.edu.tw (D.-H. Chen).

0925-8388/$ – see front matter © 2009 Elsevier B.V. All rights reserved.
doi:10.1016/j.jallcom.2009.02.017

and their properties can be tuned by varying the composition. So, in this work, we prepared the Ni–Ag alloy nanoparticles by the hydrazine co-reduction of Ni and Ag ions in ethylene glycol and investigated their EM wave absorption properties when embedded in the epoxy resin. The result indicated that Ni–Ag alloy nanoparticles indeed exhibited significant mono- or dual-frequency absorption in 2–40 GHz, depending on the composition. From the investigations on the basic properties of alloy nanoparticles as well as the frequency dependences of permittivity and permeability, it was suggested that the Ni- and Ag-rich microdomains might be formed within the Ni–Ag alloy nanoparticles. Also, the EM wave absorption properties of Ni–Ag alloy nanoparticles were affected more significantly by the composition-related microstructure than by the composition itself.

2. Experimental

2.1. Preparation of Ni–Ag alloy nanoparticles

Ni–Ag alloy nanoparticles were synthesized by the co-reduction of nickel nitrate and silver nitrate in ethylene glycol with hydrazine and polyethyleneimine (PEI) as the reducing agent and protective agent, respectively. Firstly, 0.1 M of metal precursor (500 μL/mL), 0.1 M NaOH (100 μL/mL), and 20 M hydrazine (50 μL/mL) were added into ethylene glycol in sequence and then the solution was heated to 60 °C. When the solution became grey-black which indicated the formation of Ni–Ag alloy nanoparticles, the solution was immediately cooled in an ultrasonic bath at 0 °C and PEI (5 wt%) was added to prevent the agglomeration of Ni–Ag alloy nanoparticles. After about 30 min, the product was recovered magnetically and then washed with ethanol to remove the extra ethyl glycol and PEI. Finally, the product was dried at room temperature in a vacuum oven. The total metal ion concentration was fixed at 50 mM. By varying the concentration ratio of nickel nitrate to silver nitrate, the composition of Ni–Ag alloy nanoparticles could be adjusted. In the absence of silver nitrate or nickel nitrate, pure Ni and Ag nanoparticles could be obtained, respectively. For the synthesis of pure Ag nanoparticles, the product was recovered by centrifugation.

The morphology and particle size were observed by transmission electron microscopy (TEM) using a JEOL Model JEM-1200EX transmission electron microscope at 80 kV. The structure was determined by X-ray diffraction (XRD) on a Shimadzu Model RX-III X-ray diffractometer at 40 kV and 30 mA with Cu K_α radiation ($\lambda = 0.1542$ nm). Magnetic measurement was done using a superconducting quantum interference device (SQUID) magnetometer (MPMS7, Quantum Design). The UV–vis absorption spectrum of metal colloid dispersion which was obtained by dispersing PEI-protected metal nanoparticles in ethanol was analyzed by a Hitachi U-3000 spectrophotometer equipped with a 10 mm quartz cell. The real compositions of Ni–Ag nanocrystals were determined by dissolving the sample in a concentrated HCl/HNO_3 (3:1, v/v) mixture solution and analyzing the solution composition using a GBC Model SDS-270 atomic absorption spectrometer (AAS).

2.2. Measurement of electromagnetic wave absorption property

Epoxy resin composites were prepared as follows. Firstly, reagent A and reagent B of epoxy resin were separately added into two ethanol solutions with the same content of PEI-protected metal nanoparticles. Secondly, they were ultra-sonicated to ensure the uniform dispersion and then heated to remove ethanol. When most of ethanol was evaporated, these two solutions were mixed homogeneously. Finally, by casting the mixture on a transparency film and drying in air, epoxy resin composite could be obtained. The ratio of metal nanoparticles to the epoxy resin was fixed at 4:5 by weight. The composites were cured and then cut into sheet samples of 15 cm × 15 cm with thicknesses of about 1.5 mm. The reflection loss (RL) of each sheet sample backed by the same-sized reference metal plate at frequencies of 2–18 and 18–40 GHz was measured using free space method developed by Damaskos Inc., known as free-space antenna-based inverted arch system, and a HP8722ES network analyzer. Both low band free space setup (DI Inverted Arch) and high band free space setup (DI mm-Wave Arches) were used to measure the reflection characteristics of metal-backed sheet sample at frequencies sweeping from 2 to 18 GHz and 18 to 40 GHz, respectively. Complex permittivity ε and permeability μ were determined from the scattering parameters S_{11} and S_{21} (corresponding to the scattering reflection and transmission coefficients, respectively) measured by the HP8722ES network analyzer according to the following equations [27]:

$$\varepsilon = \frac{\gamma}{\gamma_0}\left(\frac{1-\Gamma}{1+\Gamma}\right) \tag{1}$$

$$\mu = \frac{\gamma}{\gamma_0}\left(\frac{1+\Gamma}{1-\Gamma}\right) \tag{2}$$

where γ_0 is the propagation constant in free space, γ is the propagation constant in the absorber, and Γ is the reflection coefficient between air and the absorber. Γ and γ were determined in terms of S_{11} and S_{21} to be

$$\Gamma = \frac{(S_{11}^2 - S_{21}^2 + 1) \pm \sqrt{(S_{11}^2 - S_{21}^2 + 1)^2 - 4S_{11}^2}}{2S_{11}^2} \tag{3}$$

$$\gamma = -\frac{1}{d}\frac{(S_{11}^2 - S_{21}^2 + 1) \pm \sqrt{(S_{11}^2 - S_{21}^2 + 1)^2 - 4S_{21}^2}}{2S_{21}^2} \tag{4}$$

where d is the absorber thickness. From the the ratios of the permittivity and permeability of absorber (ε and μ) to the permittivity and permeability of free space (ε_0 and μ_0), relative permittivity ε_r (=$\varepsilon/\varepsilon_0$) and permeability μ_r (=μ/μ_0) could be obtained respectively. The RL curves at various frequencies and absorber thicknesses could be calculated from the relative permeability and permittivity according to the following equations [1,4,6]:

$$Z_{in} = Z_0\left(\frac{\mu_r}{\varepsilon_r}\right)^{\frac{1}{2}}\tanh\left[j\left(\frac{2\pi f d}{c}\right)(\mu_r\varepsilon_r)^{\frac{1}{2}}\right] \tag{5}$$

$$RL = 20\log\left|\frac{(Z_{in} - Z_0)}{(Z_{in} + Z_0)}\right| \tag{6}$$

where f is the frequency of electromagnetic wave, c is the velocity of light, Z_0 is the impedance of free space, and Z_{in} is the input impedance of absorber.

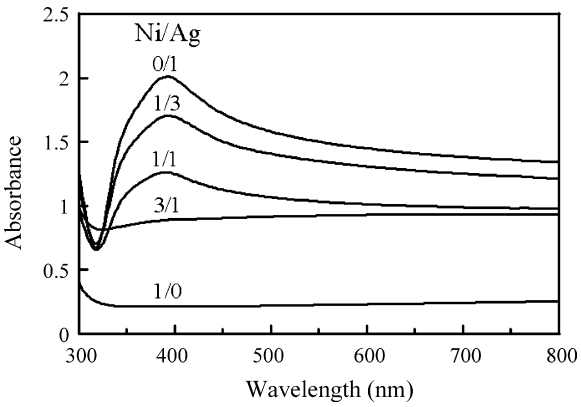

Fig. 1. UV–vis absorption spectra for the colloid dispersion of Ni, Ag, and their alloy nanoparticles with various Ni/Ag molar ratios.

3. Results and discussion

3.1. Size, structure, and optical and magnetic properties of Ni–Ag alloy nanoparticles

Fig. 1 shows the typical UV–vis absorption spectra for the colloid dispersion of Ni, Ag, and their alloy nanoparticles with various Ni/Ag molar ratios. Obviously, Ag nanoparticles exhibited their characteristic absorption band at 394 nm [28]. After incorporating Ni element, the characteristic absorption band essentially remained unchanged but the absorbance decreased significantly with the increase of Ni content. Because the nanoparticles were recovered magnetically, they must contain Ni element in each particle. Also, as illustrated in Fig. 1, Ni nanoparticles did not show any characteristic absorption in the examined wavelength range. So the characteristic absorption of nanoparticles could be attributed to the surface plasmon resonance of Ag. This provided an evidence for the formation of Ni–Ag alloy nanoparticles and revealed the electron cloud oscillation of surface Ag atoms might be perturbed by Ni atoms.

Fig. 2a–e shows the typical TEM images and particle size distributions of Ni, Ag, and their alloy nanoparticles with various Ni/Ag molar ratios. Ni_3Ag_1, Ni_1Ag_1, and Ni_1Ag_3 denote the Ni–Ag alloy nanoparticles obtained at the initial Ni/Ag molar ratios of 3/1, 1/1, and 1/3, respectively. It was obvious that they all were discrete without agglomeration. The mean diameters of Ni, Ag, Ni_3Ag_1, Ni_1Ag_1, and Ni_1Ag_3 nanoparticles were 6.5, 6.3, 6.7, 7.2, and 6.7 nm, respectively. The composition dependence of particle size was illustrated in Fig. 2f, in which the error bars indicated the standard

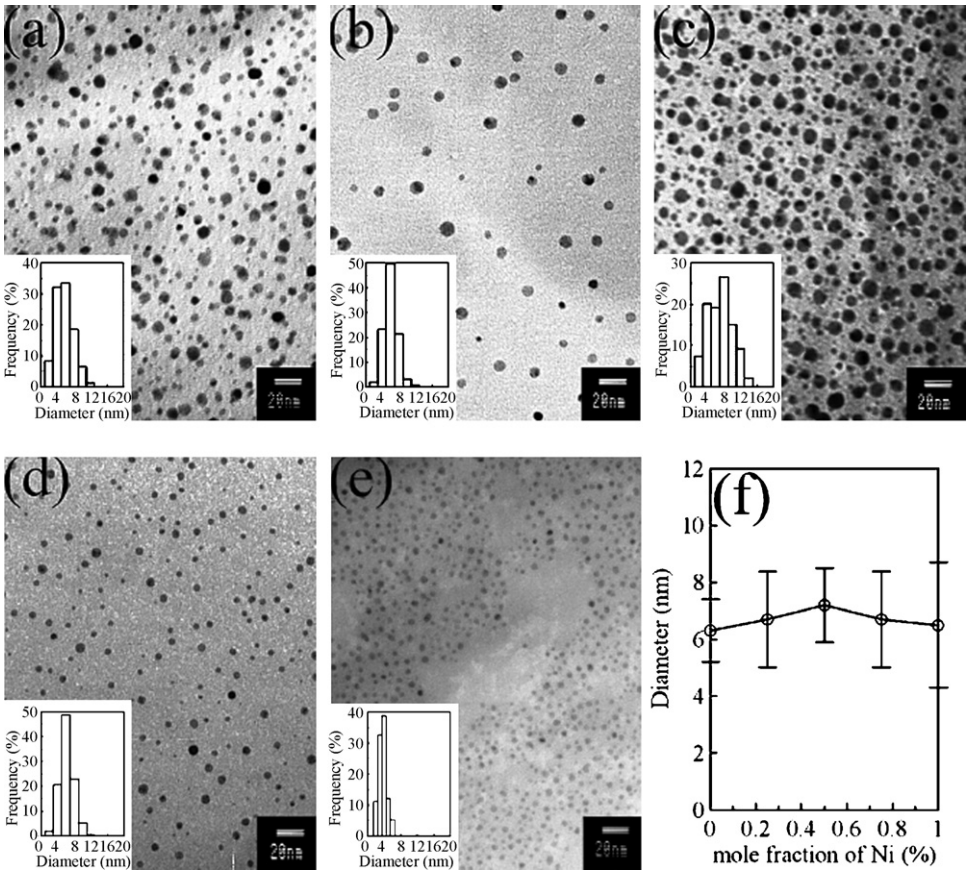

Fig. 2. Typical TEM images and particle size distributions of Ni (a), Ni_3Ag_1 (b), Ni_1Ag_1 (c), Ni_1Ag_3 (d), and Ag (e) nanoparticles and their mean diameter as a function of composition (f).

deviations. It was found that the mean diameters of Ni–Ag alloy nanoparticles were slightly larger than those of pure Ni and Ag nanoparticles and a maximum seemed to occur when the Ni/Ag molar ratio was 1. Although this effect was not remarkable while taking the particle size distribution into account, it still implied that the reduction, nucleation, and growth processes might be slightly affected by the composition of reaction solution. In addition, by AAS the real mole fractions of Ag in the products Ni_3Ag_1, Ni_1Ag_1, and Ni_1Ag_3 nanocrystals were determined to be 25.6, 56.1, and 73.5%, respectively. Because Ni–Ag alloy nanoparticles were recovered magnetically, the consistency between the real compositions and initial composition confirmed the formation of Ni–Ag alloy nanoparticles.

The XRD patterns of Ni, Ag, and their alloy nanoparticles with various Ni/Ag molar ratios were indicated in Fig. 3a. It was found that Ni nanoparticles showed three main characteristic peaks for the (1 1 1), (2 0 0) and (2 2 0) planes of face-centered cubic (fcc) Ni at 2θ=44.8, 52.2 and 76.8°. Also, Ag nanoparticles exhibited four main characteristic peaks for the (1 1 1), (2 0 0), (2 2 0), and (3 1 1) planes of fcc Ag at 2θ=38.1, 44.3, 64.4, and 77.5°. For Ni–Ag alloy nanoparticles, five characteristic peaks were observed for all of Ni_3Ag_1, Ni_1Ag_1, and Ni_1Ag_3 nanoparticles. Although the character-

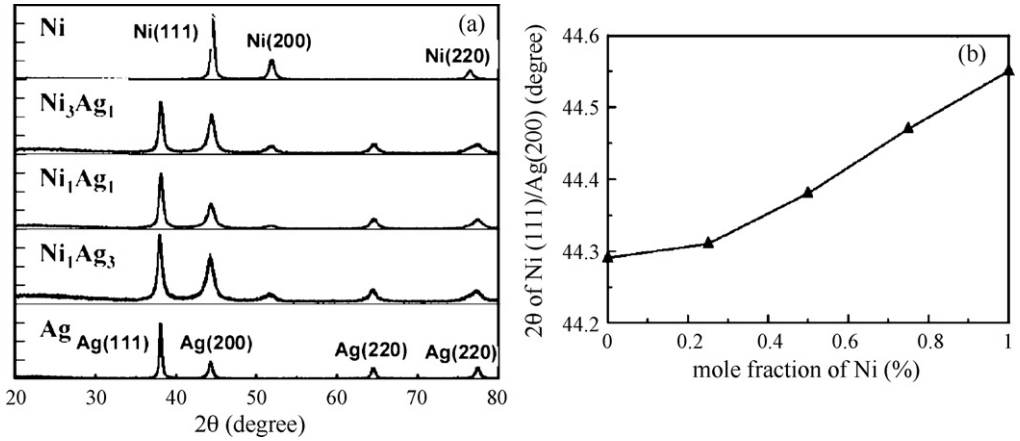

Fig. 3. XRD patterns of metal nanoparticles with various Ni/Ag molar ratios (a) and the composition dependence of the diffraction angles for Ni(1 1 1) and/or Ag(2 0 0) planes (b).

istic peaks for the (1 1 1) and (2 2 2) planes of fcc Ni were overlapped with those for the (2 0 0) and (3 1 1) planes of Ag, the (1 1 1) and (2 2 0) planes of fcc Ag and the (2 0 0) plane of fcc Ni were observed separately [29]. This confirmed the presence of Ni and Ag in the resultant alloy nanoparticles. Also, they all had the fcc structure. In addition, it was noted that the diffraction angles of Ni, Ag, and their alloy nanoparticles for Ni(1 1 1) and/or Ag(2 0 0) planes increased slightly with increasing Ni content. Their dependence on the composition was shown in Fig. 3b. According to the Vegard's law, the diffraction peak of the metal alloy with homogeneous composition should lie between the two set peaks of pure metals and change linearly [30]. Fig. 3b indicates the diffraction peak of Ni–Ag alloy nanoparticles indeed lay between those of pure Ni and Ag, revealing the formation of metal alloy. However, the composition dependence deviated from the linearity slightly, implying Ni and Ag atoms might be not homogeneously distributed throughout the bulk phase of alloy nanoparticles. This might be resulted by the differences in the reduction, nucleation, and growth rates of nickel and silver ions, consistent with the suggestion from the composition dependence of particle size [31].

Because of the presence of Ni and Ag, Ni–Ag alloy nanoparticles not only showed the surface plasmon absorption but also were expected to possess magnetic property. The typical plots of magnetization versus magnetic field (M-H loop) at 27 °C for Ni nanoparticles and the Ni–Ag alloy nanoparticles with various Ni/Ag molar ratios were indicated in Fig. 4. It was obvious that no significant hysteresis phenomenon was observed for each case. This revealed that the resultant Ni and Ni–Ag alloy nanoparticles were nearly superparamagnetic, which could be attributed to their small sizes. From Fig. 4 and its enlargement near the origin as shown in the inset, the saturation magnetization (M_s), remanent magnetization (M_r), and coercivity (H_c) could be determined. For Ni, Ni_3Ag_1, Ni_1Ag_1, and Ni_1Ag_3 nanoparticles, the M_s values were 47.8, 26.2, 18.9, and 3.1 emu/g, respectively; the M_r values were 7.7, 7.2, 2.6, and 0.9 emu/g, respectively; the H_c values were 124, 156, 94.6, and 149 Oe, respectively. It was obvious that both the M_s and M_r values decreased with the decrease in the content of Ni. This was reasonable because the magnetic property originated from the Ni element. As for the coercivity, the H_c values of Ni_3Ag_1 and Ni_1Ag_3 nanoparticles were similar but they were larger than that of Ni_1Ag_1 nanoparticles. As stated above, the differences in the reduction, nucleation, and growth rates of nickel and silver ions might lead to the inhomogeneous distribution of Ni and Ag atoms in the bulk phase of alloy nanoparticles. Also, this effect depended on the composition and might result in the variation of particle microstructure [32]. So, in addition to the experimental errors, the composition

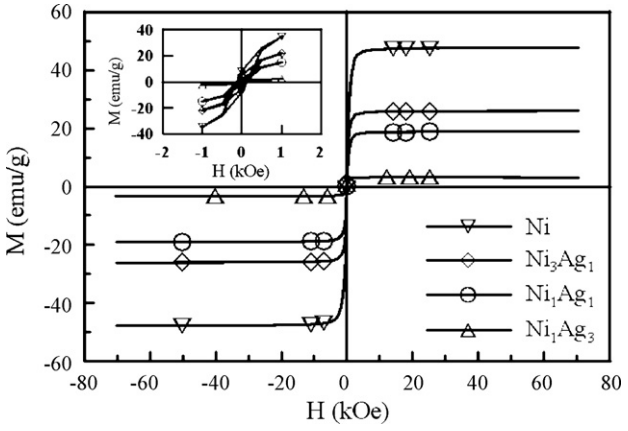

Fig. 4. Typical plots of magnetization versus magnetic field (M-H loop) at 27 °C for Ni nanoparticles and the Ni–Ag alloy nanoparticles with various Ni/Ag molar ratios. The inset indicates the enlargement near the origin.

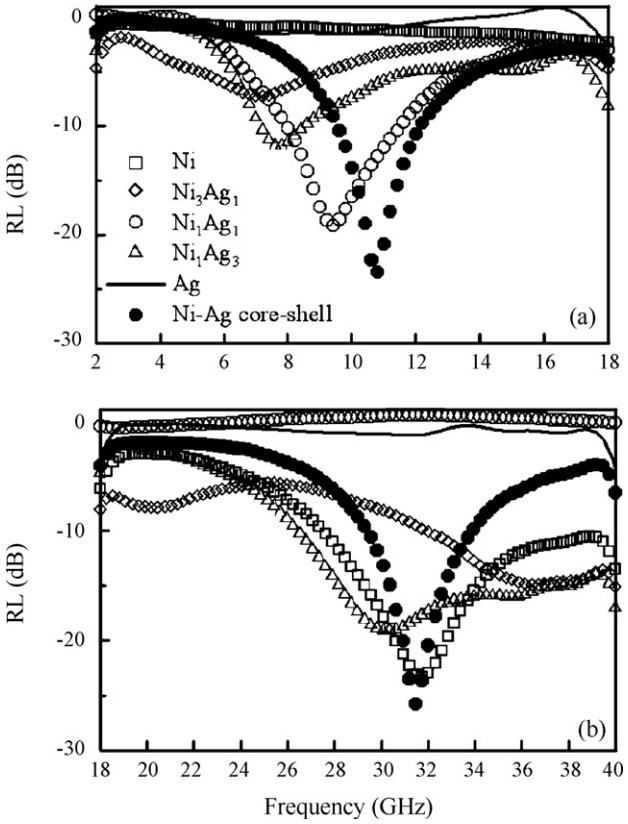

Fig. 5. Reflection loss curves for the epoxy resin composites containing Ni, Ag, and their alloy and core–shell nanoparticles in the frequency ranges of 2–18 (a) and 18–40 GHz (b).

dependence of H_c value for Ni–Ag alloy nanoparticles implied the presence of the difference in their microstructures at various Ni/Ag molar ratios.

3.2. Electromagnetic wave absorption properties of Ni–Ag nanoparticles

From the reflection measurements, the RL curves for the epoxy resin composites containing Ni–Ag alloy nanoparticles in the frequency ranges of 2–18 and 18–40 GHz were obtained as indicated in Fig. 5, in which the data for Ni, Ag and Ni–Ag core–shell nanoparticles were also given for comparison. Obviously, the EM wave absorption properties of Ni–Ag alloy nanoparticles depended on the composition. It was found that Ni_1Ag_1 nanoparticles exhibited a significant absorption as Ni nanoparticles did, but the frequency range shifted from 18–40 to 2–18 GHz with a maximum reflection loss of 19.5 dB at 9.4 GHz. Notably, both the Ni_3Ag_1 and Ni_1Ag_3 nanoparticles showed dual-frequency absorption in 2–18 and 18–40 GHz as Ni–Ag core–shell nanoparticles did [26]. For Ni_3Ag_1 nanoparticles, one maximum reflection loss of 7.3 dB at 7.1 GHz and the other maximum reflection loss of 15.0 dB at 36.5 GHz were observed. In the case of Ni_1Ag_3 nanoparticles, two maximum reflection losses of 11.7 and 18.9 dB appeared at 7.7 and 30.3 GHz, respectively. To our best knowledge, such a dual-frequency EM wave absorption property of alloy nanoparticles has not been reported. Because the composition dependences of size, diffraction angle, and coercivity all implied that Ni and Ag atoms might be not homogeneously distributed in the bulk phase of alloy nanoparticles as stated above, it was suggested that the composition dependence of the EM wave absorption properties of Ni–Ag alloy nanoparticles might be referred to the difference in their microstructures. That is, the dispersed Ni- and Ag-rich micro-domains might be formed in the bulk phases of

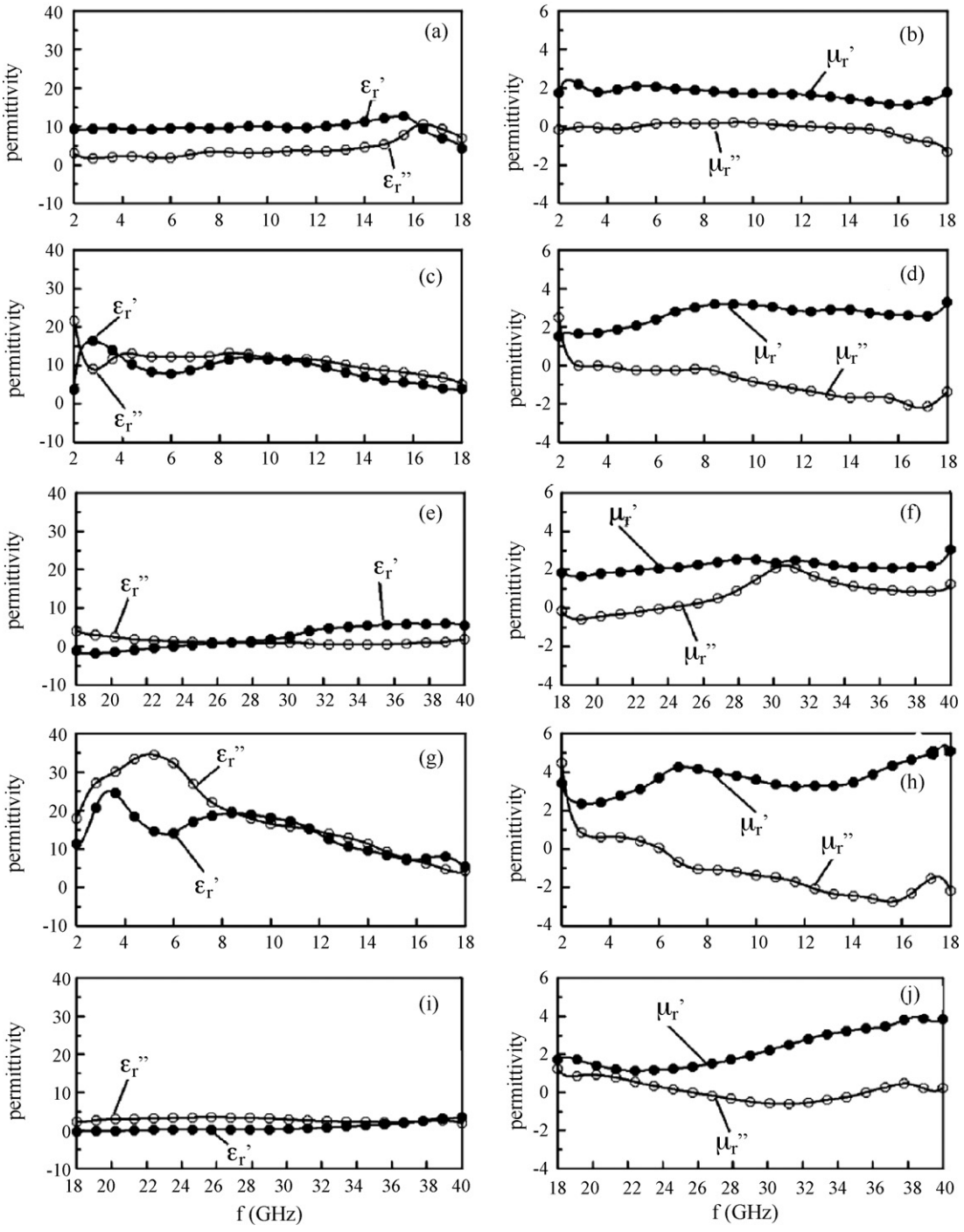

Fig. 6. Frequency dependences of the real part (ε_r' and μ_r') and imaginary part (ε_r'' and μ_r'') of the relative complex permittivity for the epoxy resin composites containing Ni_1Ag_1 (a–b), Ni_1Ag_3 (c–f), or Ni_3Ag_1 (g–j) nanoparticles.

Ni_3Ag_1 and Ni_1Ag_3 nanoparticles, respectively, which led to the appearance of the second absorption due to the lags of polarization at the interfaces as observed for Ni–Ag core–shell nanoparticles. As for the Ni_1Ag_1 nanoparticles, the distribution of Ni and Ag atoms in the bulk phase of alloy nanoparticles might be homogeneous relatively because their content was equal. So, only an absorption band was observed and the shift of absorption frequency range from 18–40 GHz to 2–18 GHz reflected the change in the nature of Ni nanoparticles after the incorporation of Ag element into their bulk phase.

The frequency dependences of the real parts (ε_r' and μ_r') and imaginary parts (ε_r'' and μ_r'') of the relative complex permittivity and permeability for the epoxy resin composites containing Ni–Ag alloy nanoparticles in the frequency ranges where they exhibited significant absorption were shown in Fig. 6. In 18–40 GHz, the frequency dependences of ε_r' and ε_r'' values for Ni_1Ag_3 and Ni_3Ag_1 nanoparticles were similar to those of Ni nanoparticles observed in our previous work [26]. Furthermore, the μ_r' values for both Ni_1Ag_3 and Ni_3Ag_1 nanoparticles were slightly higher than those for Ni nanoparticles, and the frequency at which a maximum μ_r'' value appeared was varied with the composition. Obviously, no consistent tendency was observed for the variations of μ_r', and μ_r'' values with Ni content. In 2–18 GHz, it was found that the frequency dependences of the ε_r', ε_r'', μ_r', and μ_r'' values had no significant tendencies

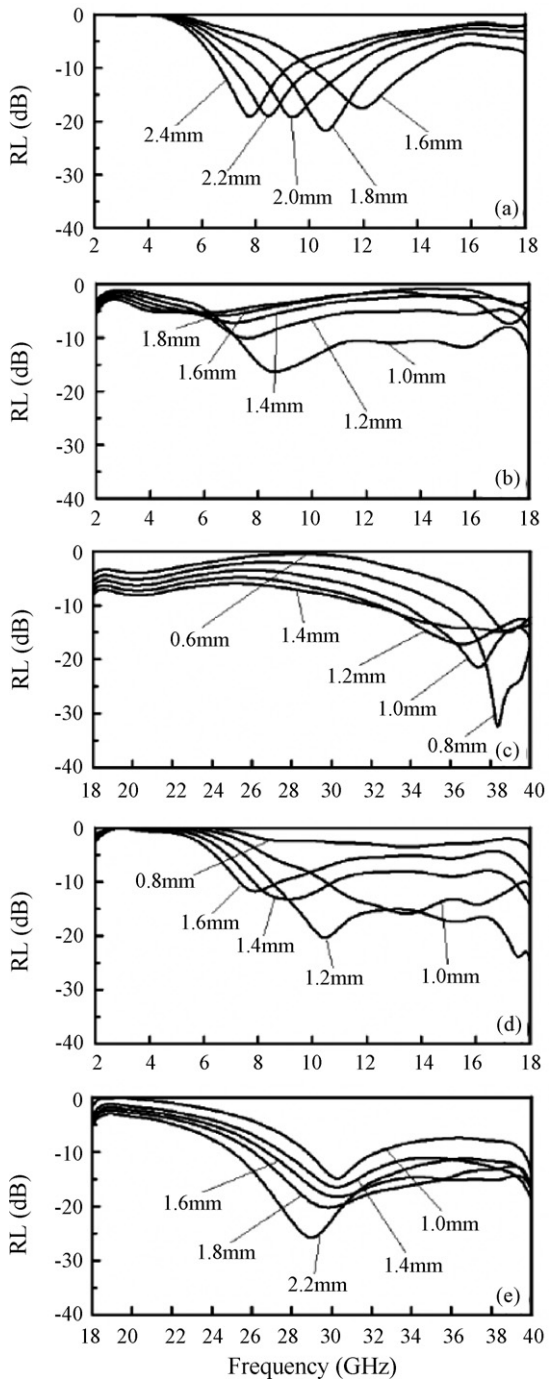

Fig. 7. Reflection loss curves for the epoxy resin composites containing Ni_1Ag_1 (a), Ni_3Ag_1 (b–c), and Ni_1Ag_3 (d–e) nanoparticles at various absorber thicknesses.

consistent with the variation of composition. In fact, the frequency dependences of the ε_r', ε_r'', μ_r', and μ_r'' values for Ni_1Ag_3 nanoparticles were more similar to those for Ni_3Ag_1 nanoparticles while comparing with Ni_1Ag_1 nanoparticles. Because the relative complex permeability and permittivity are determined not only by the nature of fillers but also by their microstructures [2,4,5], it was suggested that the composition-related microstructure as mentioned above might play a more important role than the composition itself on influencing the relative permittivity and permeability of Ni–Ag alloy nanoparticles. This result provides a new idea for the design or development of alloy nanoparticles-based EM wave absorption materials.

Furthermore, it was noted that negative μ_r'' values were observed in some conditions as indicated in Fig. 6. Similar phenomenon was also found in our previous work [26]. This might be meaningless in physics because these values were obtained by simulation based on the scattering parameters and the negative values might have just arisen from noise or experimental artifice. However, theoretically, the metallic magnetic nanoparticles might be used as the material with negative reflection (so called left-handed materials) whose permittivity and permeability were negative [33–38]. So, this also might imply that Ni–Ag alloy nanoparticles had the potential as the left-handed materials. More studies and precise measurement were necessary.

The layer thickness of absorbers is also an important factor influencing the shielding efficiency of absorbers. According to equations (5) and (6), the RL curves for the epoxy resin composites containing Ni–Ag alloy nanoparticles at various thicknesses in the frequency where they exhibited significant absorption could be calculated as indicated in Fig. 7. For Ni_1Ag_1 nanoparticles, a maximum reflection loss of 21.7 dB at 10.6 GHz appeared at an absorber thickness of 1.8 mm. For Ni_3Ag_1 nanoparticles, a maximum reflection loss of 16.3 dB at 8.6 GHz appeared at an absorber thickness of 1.0 mm and a maximum reflection loss of 32.4 dB at 38.4 GHz at an absorber thickness of 0.8 mm. For Ni_1Ag_3 nanoparticles, a maximum reflection loss of 20.3 dB at 10.5 GHz appeared at an absorber thickness of 1.2 mm and a maximum reflection loss of 25.7 dB at 29.0 GHz at an absorber thickness of 2.2 mm.

4. Conclusions

Discrete Ni–Ag alloy nanoparticles with various molar ratios have been synthesized by the co-reduction of nickel nitrate and silver nitrate in ethylene glycol with hydrazine and PEI as the reducing agent and protective agent, respectively. They showed the surface plasmon absorption at 394 nm and were nearly superparamagnetic, with the fcc structure and the mean diameters of 6.3–7.2 nm. From the composition dependences of size, diffraction angle, and magnetic property, it was suggested that Ni and Ag atoms might not be homogeneously distributed in the bulk phase of composite nanoparticles due to the differences in the reduction, nucleation, and growth rates of nickel and silver ions. From the measurement of the reflection loss in 2–18 and 18–40 GHz, it was found that Ni_1Ag_1 nanoparticles exhibited a significant absorption as Ni nanoparticles did, but both the Ni_3Ag_1 and Ni_1Ag_3 nanoparticles showed dual-frequency absorption as Ni–Ag core–shell nanoparticles did. It was suggested that Ni- and Ag-rich micro-domains might be formed in the bulk phases of Ni_3Ag_1 and Ni_1Ag_3 nanoparticles, respectively, but the distribution of Ni and Ag atoms in the bulk phase of Ni_1Ag_1 nanoparticles might be homogeneous relatively. The presence of dispersed micro-domains might result in the lags of polarization at the interfaces as the frequency was varied, and lead to the appearance of an additional absorption band which contributed to the dielectric loss. In addition, it was suggested that the permittivity and permeability of Ni–Ag nanoparticles were affected more significantly by the composition-related microstructure than by the composition itself. This result should be helpful for the development of multi-frequency EM wave absorption materials.

Acknowledgments

We are grateful to the Chung-Shan Institute of Science & Technology for the financial and technical support of this research (contract no. XD95026P), and to Dr. Jenq-Der Tsou for his valuable knowledge on this work.

References

[1] J.R. Liu, M. Itoh, T. Horikawa, E. Taguchi, H. Mori, K. Machida, Appl. Phys. A 82 (2006) 509–513.
[2] Y. Deng, L. Zhao, B. Shen, L. Liu, W. Hu, J. Appl. Phys. 100 (2006) 14304.
[3] A. Ghasemi, A. Hossienpour, A. Morisako, A. Saatchi, M. Salehi, J. Magn. Magn. Mater. 302 (2006) 429–435.
[4] J.R. Liu, M. Itoh, K.I. Machida, Appl. Phys. Lett. 88 (2006) 62503.
[5] X.F. Zhang, X.L. Dong, H. Huang, Y.Y. Liu, W.N. Wang, X.G. Zhu, B. Lv, J.P. Lei, C.G. Lee, Appl. Phys. Lett. 89 (2006) 53115.
[6] S. Sun, C.B. Murray, D. Weller, L. Folks, A. Moser, Science 287 (2000) 1989–1992.
[7] M.L. Wu, D.H. Chen, T.C. Huang, Chem. Mater. 13 (2001) 599–606.
[8] M.A. Malik, P. O'Brien, N. Revaprasadu, Chem. Mater. 14 (2002) 2004–2010.
[9] T. Gao, Q. Li, T. Wang, Chem. Mater. 17 (2005) 887–892.
[10] T. Hirakawa, P.V. Kamat, J. Am. Chem. Soc. 127 (2005) 3928–3934.
[11] X. Su, J. Zhang, L. Sun, T.W. Koo, S. Chan, N. Sundararajan, M. Yamakawa, A.A. Berlin, Nano Lett. 5 (2005) 49–54.
[12] F. Caruso, Adv. Mater. 13 (2001) 11–22.
[13] C.M. Niemeyer, Angew. Chem. Int. Ed. 40 (2001) 4128–4158.
[14] Y. Lu, Y. Yin, B.T. Mayers, Y. Xia, Nano Lett. 2 (2002) 183–186.
[15] S.T. Selvan, J.P. Spatz, H.A. Klok, M. Möller, Adv. Mater. 10 (1998) 132–134.
[16] M.M. Natile, A. Glisenti, Chem. Mater. 17 (2005) 3403–3413.
[17] D. Pan, Q. Wnag, S. Jiang, X. Ji, L. An, Adv. Mater. 17 (2005) 176–179.
[18] J. Jang, Y. Nam, H. Yoon, Adv. Mater. 17 (2005) 1382–1386.
[19] W. Yang, H. Araki, C. Tang, S. Thaveethavorn, A. Kohyama, H. Suzuki, T. Noda, Adv. Mater. 17 (2005) 1519–1523.
[20] S. Zhou, B. Varughese, B. Eichhorn, G. Jackson, K. McIlwrath, Angew. Chem. Int. Ed. 44 (2005) 4539–4543.
[21] D.H. Chen, S.H. Wu, Chem. Mater. 12 (2000) 1354–1360.
[22] D.H. Chen, C.H. Hsieh, J. Mater. Chem. 12 (2002) 2412–2415.
[23] S.H. Wu, D.H. Chen, J. Colloid. Interface Sci. 259 (2003) 282–286.
[24] S.H. Wu, D.H. Chen, Chem. Lett. 33 (2004) 406–407.
[25] C.C. Lee, D.H. Chen, Nanotechnology 17 (2006) 3094.
[26] C.C. Lee, D.H. Chen, Appl. Phys. Lett. 90 (2007) 193102.
[27] B.T. Lee, H.C. Kim, Jpn. J. Appl. Phys. 35 (1996) 3401–3406.
[28] D.H. Chen, C.J. Chen, J. Mater. Chem. 12 (2002) 1557–1562.
[29] J. Xu, T. Klassen, R.S. Averback, J. Appl. Phys. 79 (1996) 3935–3945.
[30] B.Y. Tsaur, M. Maenpaa, J. Appl. Phys. 52 (1981) 728–736.
[31] B.J. Hwang, L.S. Sarma, J.M. Chen, C.H. Chen, S.C. Shih, G.R. Wang, D.G. Liu, J.F. Lee, M.T. Tang, J. Am. Chem. Soc. 127 (2005) 11140–11145.
[32] S. Bedanta, W. Kleemann, J. Phys. D: Appl. Phys. 42 (2009) 013001.
[33] J.B. Pendry, A.J. Holden, W.J. Stewart, I. Youngs, Phys. Rev. Lett. 76 (1996) 4773–4776.
[34] R.A. Shelby, D.R. Smith, S. Schultz, Science 292 (2001) 77–79.
[35] R.A. Shelby, D.R. Smith, S.C. Nemat-Nasser, S. Schultz, Appl. Phys. Lett. 78 (2001) 489–491.
[36] D.R. Smith, W.J. Padilla, D.C. Vier, S.C. Nemat-Nasser, S. Schultz, Phys. Rev. Lett. 84 (2000) 4184–4187.
[37] S.T. Chui, L. Hu, Phys. Rev. B 65 (2002) 144407.
[38] T. Kasagi, T. Tsutaoka, K. Hatakeyama, Appl. Phys. Lett. 88 (2006) 172502.